nature genetics

LIN28B induces neuroblastoma and enhances MYCN levels via *let-7* suppression

Jan J Molenaar[1], Raquel Domingo-Fernández[2,3], Marli E Ebus[1], Sven Lindner[4], Jan Koster[1], Ksenija Drabek[1], Pieter Mestdagh[5], Peter van Sluis[1], Linda J Valentijn[1], Johan van Nes[1], Marloes Broekmans[1], Franciska Haneveld[1], Richard Volckmann[1], Isabella Bray[2,3], Lukas Heukamp[6], Annika Sprüssel[4], Theresa Thor[4], Kristina Kieckbusch[4], Ludger Klein-Hitpass[7], Matthias Fischer[8], Jo Vandesompele[5], Alexander Schramm[4], Max M van Noesel[9], Luigi Varesio[10], Frank Speleman[5], Angelika Eggert[4], Raymond L Stallings[2,3], Huib N Caron[1], Rogier Versteeg[1] & Johannes H Schulte[4]

LIN28B regulates developmental processes by modulating microRNAs (miRNAs) of the *let-7* family. A role for LIN28B in cancer has been proposed but has not been established *in vivo*. Here, we report that *LIN28B* showed genomic aberrations and extensive overexpression in high-risk neuroblastoma compared to several other tumor entities and normal tissues. High *LIN28B* expression was an independent risk factor for adverse outcome in neuroblastoma. LIN28B signaled through repression of the *let-7* miRNAs and consequently resulted in elevated MYCN protein expression in neuroblastoma cells. LIN28B–let-7–MYCN signaling blocked differentiation of normal neuroblasts and neuroblastoma cells. These findings were fully recapitulated in a mouse model in which LIN28B expression in the sympathetic adrenergic lineage induced development of neuroblastomas marked by low *let-7* miRNA levels and high MYCN protein expression. Interference with this pathway might offer therapeutic perspectives.

LIN28 and its homolog LIN28B are proteins that bind small RNA and are highly expressed in stem cells and developing tissues[1]. They regulate germ cell development, skeletal myogenesis and neurogenesis[2–4] but also influence metabolic processes, such as insulin sensitivity and glucose uptake[5]. LIN28 is known to be a master regulator of pluripotency in embryonic stem cells. In combination with NANOG, OCT4 and SOX2, it can reprogram differentiated cells to pluripotent stem cells[6].

Both *LIN28* and *LIN28B* may contribute to the development of several types of cancer. Rare amplifications in these genes and/or overexpression have been reported in hepatocellular carcinoma (HCC), leukemia, Wilms' tumor and a variety of other malignancies[7–9]. Overexpression was found to mediate cellular transformation, and targeted silencing in cancer cell systems induced differentiation. High expression of these genes was associated with advanced disease and poor outcome[7,10,11]. Genome-wide association studies have implicated the human *LIN28B* locus in the regulation and timing of menarche[12,13].

LIN28 and LIN28B function as negative regulators of miRNA biogenesis, selectively blocking the processing of *let-7* miRNA precursor molecules into mature miRNAs[14]. Most miRNAs are transcribed by RNA polymerase II as pri-miRNAs. These pri-miRNAs are processed by Drosha with the aid of Pasha to generate pre-miRNAs, which are exported from the nucleus and processed by Dicer to form mature miRNAs[15,16]. LIN28 and LIN28B inhibit the processing of *let-7* family miRNAs but act in different ways. They both bind to the unique sequences in the terminal loop of *let-7* miRNAs. LIN28 functions in the cytoplasm by recruiting TUTase to *let-7* precursors, thereby affecting Dicer-mediated processing[17–19]. LIN28B sequesters primary *let-7* transcripts in the nucleus and inhibits Drosha processing[20].

The let-7 miRNAs are a family of 12 sequence-related miRNAs that are distributed over 8 genomic clusters and are often downregulated in cancer[21]. The let-7 miRNAs function as tumor suppressors through the silencing of key oncogenes, such as *RAS*, *MYC* and *CDK6* (refs. 22–24). In some cancers, *let-7* family members seem to be downregulated[25]. Loss or low expression of *let-7* family members has prognostic value for patient survival in several cancer types[26,27].

Neuroblastoma is a childhood cancer that originates from neural crest–derived cells[28]. Neuroblastomas account for 15% of pediatric cancer deaths[29]. Approximately 20% of neuroblastomas harbor *MYCN* amplifications, a feature that is correlated with adverse clinical outcome[30]. Emerging evidence suggests a role for aberrant miRNA regulation in neuroblastoma. Expression profiling of miRNAs in neuroblastoma identified miRNA expression signatures

[1]Department of Oncogenomics, Academic Medical Center, Amsterdam, The Netherlands. [2]Department of Molecular and Cellular Therapeutics, Royal College of Surgeons in Ireland, Dublin, Ireland. [3]National Children's Research Centre, Dublin, Ireland. [4]Department of Pediatric Oncology and Haematology, Children's Hospital Essen, Essen, Germany. [5]Center for Medical Genetics, Ghent University, Ghent, Belgium. [6]Institute of Pathology, University Hospital Cologne, Cologne, Germany. [7]Institute of Cell Biology, University Hospital Essen, Essen, Germany. [8]Department of Pediatric Oncology and Hematology, Children's Hospital, University of Cologne, Cologne, Germany. [9]Department of Pediatric Oncology/Hematology, Erasmus Medical Centre–Sophia Children's Hospital, Rotterdam, The Netherlands. [10]Laboratory of Molecular Biology, Gaslini Institute, Genoa, Italy. Correspondence should be addressed to J.J.M. (j.j.molenaar@amc.uva.nl).

Received 27 March; accepted 12 September; published online 7 October 2012; doi:10.1038/ng.2436

that are predictive of clinical outcome[31–33]. Overexpression of MYCN was found to induce expression of the *miR-17-72* cluster and *miR-9*, which are known to be tumor-driving miRNAs[34–36]. The genes encoding *miR34-a* at 1p36 and *miR-125b* at 11q24 are frequently deleted and have been shown to function as tumor suppressors in neuroblastoma[37–40]. A recent study showed let-7e–mediated regulation of MYCN expression in a *MYCN*-amplified neuroblastoma cell line, and let-7e was able to inhibit proliferation and growth when overexpressed in these cells[41].

Although there is a substantial amount of literature implicating a role for *LIN28* and *LIN28B* in oncogenic processes, there is no formal proof that these genes are indeed oncogenes. In this study, we show high-level genomic amplifications of *LIN28B* and its overexpression in the majority of high-risk neuroblastoma tumors. We show that LIN28B suppresses *let-7* family miRNA expression in neuroblastoma cells, which results in increased MYCN protein levels. Overexpression of *LIN28B* in non-malignant neuroblasts was found to drive proliferation. Overexpression of *Lin28b* in neuroblasts in a transgenic mouse model caused neuroblastoma tumors with N-myc overexpression and all characteristics of human neuroblastoma, providing proof of the oncogenic role of *LIN28B* in neuroblastoma.

RESULTS

Amplification and overexpression of LIN28B in neuroblastoma

We identified a new amplified region on chromosome 6q21 in 3 high-risk neuroblastoma tumors by array–comparative genomic hybridization (aCGH) analysis of 263 tumors (**Fig. 1a** and **Supplementary Table 1**). Southern blot hybridization with a probe for 6q21 confirmed high-level amplification in the index tumor (**Supplementary Fig. 1a**). The smallest region of overlap (SRO) encompassed four genes, including *LIN28B*. Affymetrix mRNA analysis showed *LIN28B* overexpression in three independent neuroblastoma tumor series compared to normal reference tissues and a series of tissues from other malignancies (**Fig. 1b**). Notably, there was very high expression of *LIN28B* in this pediatric tumor. Some expression was seen in HCC tumors, which are known to overexpress *LIN28B*. Analysis of *LIN28B* expression[42] showed pronounced overexpression in the tumors with *LIN28B* amplification (**Supplementary Fig. 2**). Kaplan-Meier analyses showed that high expression of *LIN28B* was significantly associated with poor overall survival in 2 cohorts of 88 and 283 individuals with neuroblastoma (**Fig. 1c** and **Supplementary Figs. 1** and **2**). In multivariate analysis, high *LIN28B* expression remained a risk factor for adverse outcome independent of International Neuroblastoma Staging System (INSS)

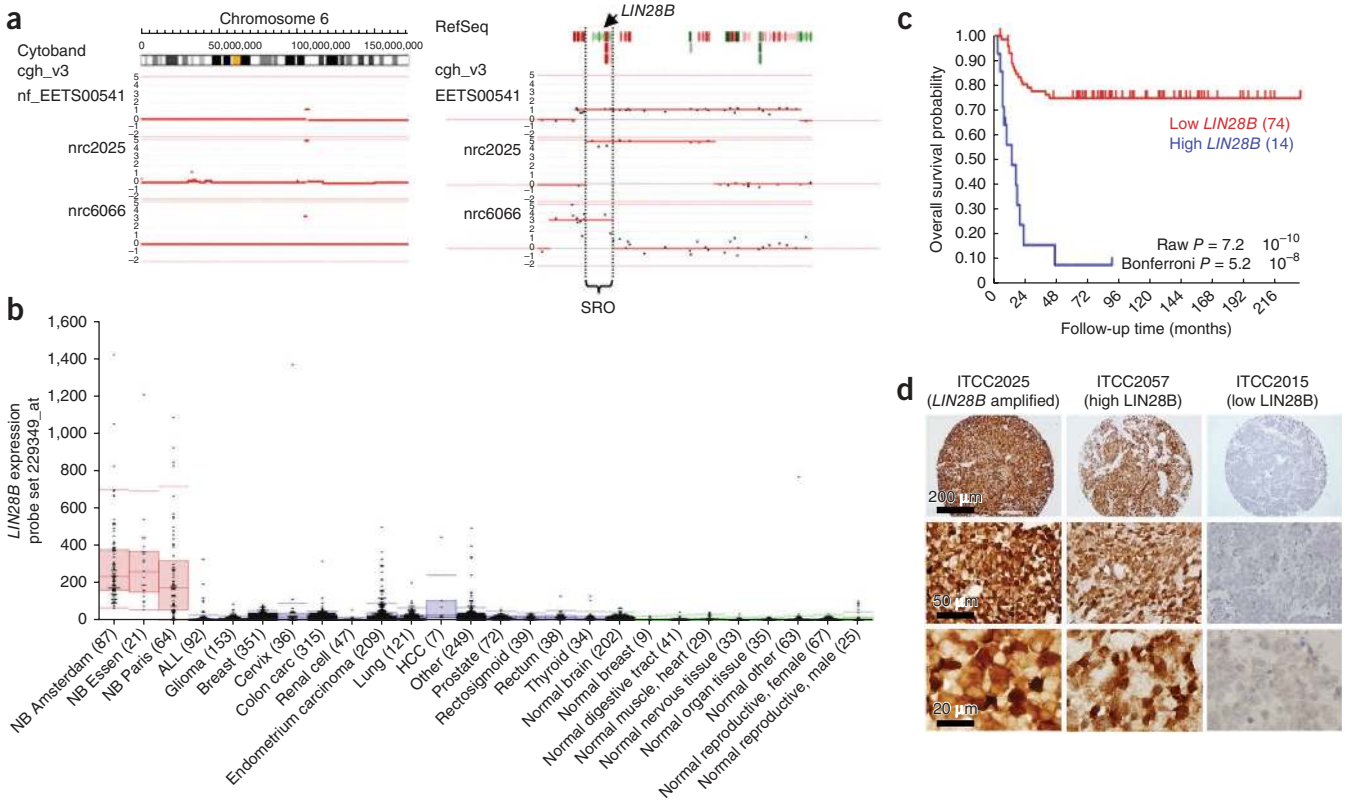

Figure 1 Amplification and overexpression of LIN28B in poor-prognosis neuroblastoma. (**a**) aCGH analysis of three tumors with amplification of the 6q21 region. Binary segmentation data are shown on a $\log_2$ scale using the R2 web application. Left, complete chromosome 6 with small amplified regions at 6q21. Right, the *LIN28B* gene locus and SRO for the three amplifications. Tumor numbers are indicated on the left. Red and green boxes indicate gene loci. (**b**) Combined box dot plot of Affymetrix mRNA expression analysis (probe set 229349_at) in three independent series of neuroblastoma tumor samples (red), series of various other tumor types (blue) and several series of normal tissues (green). The boxes indicate where 50% of the data points are located, with the upper border at 75% and the lower border at 25%. Error bars indicate the range of expression, with a maximum of 2 × the box size. The numbers in parentheses indicate the number of tumors. (**c**) Kaplan-Meier curve indicating survival of individuals with high and low expression of *LIN28B*. The cutoff was determined using the Kaplan scanner tool in the R2 web application. Samples are sorted according to the expression of *LIN28B* and divided into two groups on the basis of a cutoff expression value. All cutoff expression levels and the resulting groups were analyzed for survival, with the provision that each group include at least eight samples. For each cutoff level and grouping, the log-rank significance of projected survival was calculated. The graph depicts the best *P* value corrected for multiple testing (Bonferroni correction). Numbers in parentheses indicate the number of individuals in each group. (**d**) Neuroblastoma tissue arrays stained with an antibody to LIN28B. A tumor with genomic amplification of *LIN28B*, a tumor with typical high expression of LIN28B and a tumor with low expression of LIN28B are shown.

stage, age and the presence of *MYCN* amplification or *ALK* mutation (**Supplementary Tables 2** and **3**). LIN28B protein levels were measured by immunostaining neuroblastoma tissue arrays with 48 samples from the NB88 series, and we found a good correlation between mRNA and protein levels (**Supplementary Fig. 3**). LIN28B protein was detected in the cytoplasm as well as in the nucleus (**Fig. 1d** and **Supplementary Fig. 3**), where it is reported to be functional[20]. The frequency of high-level genomic amplification of the *LIN28B* gene locus was low but underscores the key role of very high LIN28B mRNA and protein levels in a large proportion of aggressive neuroblastomas. Taken together, these findings point to a possible oncogenic role for *LIN28B* in neuroblastoma.

Silencing *LIN28B* triggers neuronal differentiation

To validate a functional role for LIN28B overexpression, we silenced *LIN28B* using two lentiviral short hairpin RNA (shRNA) constructs targeting the mRNA coding sequence and 3′ UTR of *LIN28B*. In the neuroblastoma cell line SK-N-BE, which has LIN28B overexpression, the shRNAs caused effective degradation of *LIN28B* mRNA (**Fig. 2a**), resulting in decreased protein levels (**Fig. 2b**). Two other cell lines with high *LIN28B* expression (IMR-32 and NGP) showed similarly effective silencing of *LIN28B* (**Supplementary Fig. 4**). Downregulation of *LIN28B* produced a change in cell morphology indicative of neuronal differentiation (axon outgrowth) and resulted in a significant decrease in cell viability (**Fig. 2c**,**d**). Fluorescence-activated cell sorting (FACS) analysis after *LIN28B* knockdown indicated cell cycle growth arrest in G1 compared to control samples (**Fig. 2e**). We could not detect increased PARP cleavage or induction of a sub-G1 phase through FACS analysis, indicating that silencing of *LIN28B* did not result in apoptosis *in vitro* (data not shown). For further validation of neuronal differentiation, we performed Affymetrix mRNA profiling at various time points after *LIN28B* silencing in the SK-N-BE cell line. The gene ontology (GO) category that showed the most significant enrichment for regulated genes ($P = 3.9 \times 10^{-17}$) was that of neuropeptide hormone activity, containing the genes *NPY*, *NFASC*, *VIP* and *VGF* (**Supplementary Fig. 3**). The upregulation of these genes in response to *LIN28B* silencing could represent differentiation into a neuroendocrine lineage. These results suggest a functional dependence on LIN28B signaling in neuroblastoma cancer cells.

LIN28B regulates the *let-7* miRNA cluster

LIN28B has been reported to inhibit the processing of *let-7* family precursors to mature miRNAs[14]. To determine whether this mechanism exists in neuroblastoma cells, we first investigated the effects of targeted silencing of *LIN28B* by using lentiviruses to transduce shRNA into SK-N-BE cells (**Fig. 2a**). The same RNA pool was used for quantitative RT-PCR (qRT-PCR) analysis of expression from the miRNA genes, using primers targeting *let-7a*, *let-7e*, *let-7g*, *let-7i* and *miR-98*. Expression of all miRNAs was significantly higher in cells with targeted *LIN28B* silencing (**Fig. 3a**). Next, we investigated the effect of LIN28B overexpression in SK-N-FI cells, a cell line with low endogenous LIN28B expression. SK-N-FI cells that overexpressed LIN28B were generated with a doxycycline-inducible *LIN28B* expression vector. The cells showed basal expression of the *LIN28B* construct (incomplete repression) and strong LIN28B induction after exposure to doxycycline. Overexpression of LIN28B resulted in repression of the *let-7* miRNA cluster (**Fig. 3b**). These findings confirm an inverse relationship between LIN28B and *let-7* miRNAs in neuroblastoma cells. To determine whether this inverse correlation also exists in neuroblastoma tumors, we analyzed high-throughput mRNA and miRNA profiling data from 78 primary neuroblastoma tumors. The *LIN28B* mRNA levels, as measured by Affymetrix 133 plus 2 arrays, were used to search for inversely expressed miRNAs in a panel of 430 miRNAs assessed by qRT-PCR. Six out of eight of the miRNAs with the most significant inverse correlation with *LIN28B* belonged to the *let-7* cluster (**Supplementary Fig. 5** and **Supplementary Table 4**). These findings were confirmed in a second data set containing 200 tumors with mRNA expression data (Affymetrix Exon St 1.0 chip) and corresponding miRNA profiling data (**Supplementary Fig. 5** and **Supplementary Table 5**). Our results show that expression of the *let-7* miRNAs is downregulated by LIN28B in neuroblastoma cell lines. The inverse correlation between *LIN28B* and these miRNAs in neuroblastoma

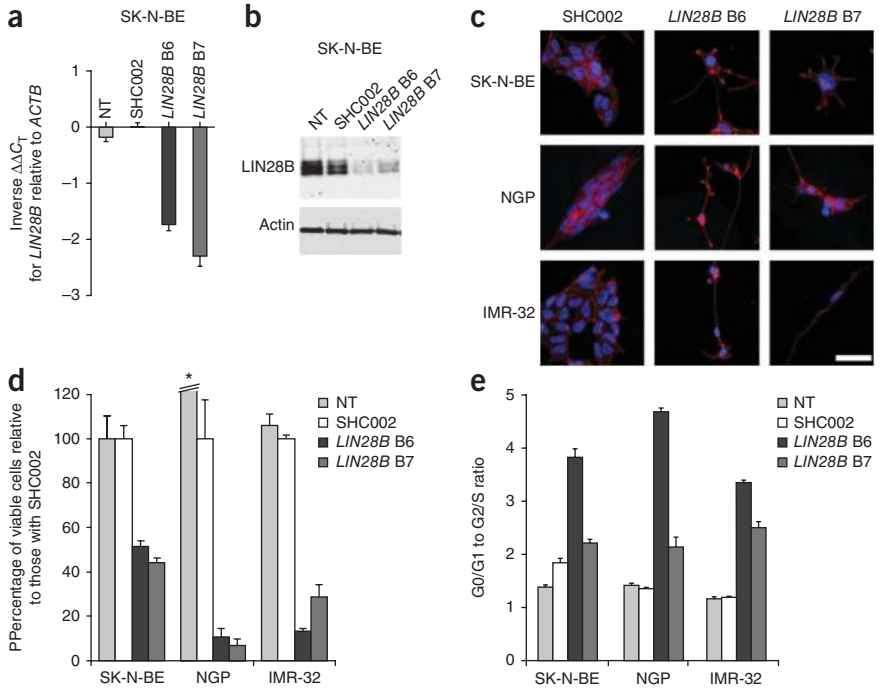

Figure 2 *LIN28B* silencing results in growth inhibition and neuronal differentiation. (**a**) qPCR analysis after *LIN28B* silencing in SK-N-BE cells. Cells were transduced with control shRNA (SHC002) or with *LIN28B* shRNA B6 or B7, and we included a non-transfected (NT) control sample. Total RNA was harvested at 72 h, and qPCR was performed to measure *LIN28B* expression. Error bars, s.d. of three independent assays. (**b**) Protein blot analysis of *LIN28B* silencing in SK-N-BE cells. Cells were harvested 72 h after infection. (**c**) Phalloidin staining of SK-N-BE, NGP and IMR-32 cells after *LIN28B* silencing. Images were acquired before harvesting for protein analysis. Scale bar, 20 µm. (**d**) MTT assay after *LIN28B* knockdown in SK-N-BE, NGP and IMR-32 cells. Cells were harvested 144 h after infection. *, value for non-transfected NGP cells of 242%. Error bars, s.d. of three independent measurements. (**e**) FACS analysis after *LIN28B* knockdown in SK-N-BE, NGP and IMR-32 cells. Bar plots indicate the number of cells in G1 and G0 phase divided by the number of cells in G2 and S phase. Error bars, s.d. from three independent experiments.

tumors strongly suggests that this mechanism is functional *in vivo*. Also, *miR-125b* showed an inverse correlation with *LIN28B* mRNA expression *in vivo*, which is a result of *LIN28B* being a direct target of miR-125b (**Supplementary Fig. 6**).

LIN28B increases MYCN protein levels

The regulation of *let-7* miRNAs by LIN28B raised the question of which genes were subsequently regulated by these miRNAs. Previously reported target genes of *let-7* signaling include *RAS*, *CDK6* and *MYC*[22–24]. To identify downstream target genes of the LIN28B–let-7 axis in neuroblastoma, we harvested protein from SK-N-BE cells at various time points after silencing *LIN28B*. Protein blot analysis with a pan-RAS antibody, which recognizes HRAS, KRAS and NRAS, and an antibody to CDK6 showed no clear correlation of protein levels with *LIN28B* silencing. However, a strong correlation between *LIN28B* silencing and the amount of MYCN protein indicated that *MYCN* is a target gene of LIN28B–let-7 signaling (**Supplementary Fig. 7**). The lower MYCN protein levels after targeted silencing of *LIN28B* did not result from reduced *MYCN* mRNA levels (**Supplementary Fig. 8**), suggesting that *MYCN* was inhibited at the level of translation. Targeted silencing of *LIN28B* was also performed in the neuroblastoma cell lines IMR-32, NGP and Kelly, which showed consistently lower levels of MYCN after *LIN28B* silencing (**Fig. 3c**). To exclude the possibility that these findings resulted from off-target effects of the *LIN28B* shRNAs, we generated SK-N-BE cells with doxycycline-inducible overexpression of the coding sequence of *LIN28B*. The *LIN28B* B6 shRNA targets the 3′ UTR of *LIN28B* and therefore cannot silence the ectopically expressed *LIN28B* construct. MYCN downregulation after silencing of *LIN28B* by the *LIN28B* B6 shRNA was rescued by ectopic overexpression of the coding region of *LIN28B*, confirming that lower amounts of MYCN protein did not result from off-target effects of the shRNA (**Fig. 3d**).

We also investigated whether LIN28B can increase MYCN protein levels in neuroblastoma cells with low endogenous *LIN28B* expression. The cell line SK-N-FI has low *LIN28B* mRNA levels and substantial *MYCN* expression but shows only low amounts of MYCN protein (**Supplementary Fig. 9**). SK-N-FI cells transfected with an inducible expression vector for *LIN28B* had higher LIN28B expression, which was further increased after doxycycline treatment. Overexpression of *LIN28B* resulted in a strong increase in the amounts of MYCN protein (**Fig. 3e**). In contrast, overexpression of *LIN28B* in SK-N-AS cells, a cell line that did not express *LIN28B*, *MYCN* or *MYC* mRNA, did not result in induction of MYCN and had no effect on cell phenotype (**Supplementary Fig. 10**).

To address the relevance of MYCN as a functional downstream target of LIN28B, we performed rescue experiments. We used a SK-N-BE subclone in which ectopic expression of *MYCN* can be induced by doxycycline. Ectopically expressed *MYCN* mRNA lacks UTR sequences and is therefore not suppressed by LIN28B-regulated miRNAs. With expression of ectopic MYCN, which resulted in higher MYCN levels after *LIN28B* knockdown relative to cells lacking ectopic MYCN expression, reduction in cell viability was strongly attenuated, and no signs of neuronal differentiation were observed (**Fig. 3f** and **Supplementary Fig. 11**). Consistently, no change in phenotype was observed with knockdown of *LIN28B* in the mouse neuroblastoma cell line NHO2A, which expresses ectopic MYCN that is not sensitive to regulation by LIN28B (**Supplementary Fig. 12**). These experiments strongly suggest that LIN28B exerts its effects mainly through the regulation of MYCN.

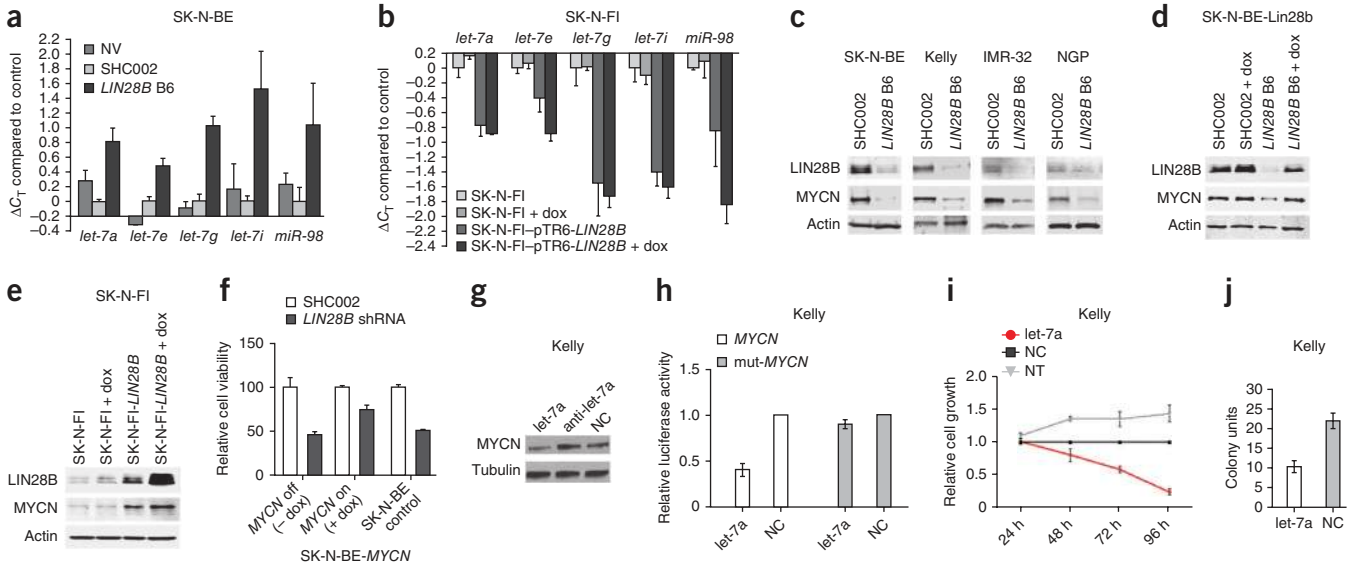

Figure 3 The LIN28B–let-7–MYCN axis in neuroblastoma. (**a**) qRT-PCR of SK-N-BE RNA 72 h after *LIN28B* silencing with primers targeting *let-7* miRNAs. NV, no virus. (**b**) qRT-PCR of *let-7* miRNAs after overexpression of *LIN28B* in SK-N-FI cells with and without doxycycline (dox). (**c**) Protein blots of samples harvested 72 h after *LIN28B* silencing in SK-N-BE, Kelly, IMR-32 and NGP cells. (**d**) Protein blots of *LIN28B* knockdown rescue in SK-N-BE cells with inducible ectopic *LIN28B* overexpression. Cells with and without doxycycline were treated for 72 h with *LIN28B* B6 shRNA, which does not target ectopically expressed *LIN28B*. (**e**) Protein blot of SK-N-FI cells and SK-N-FI cells transfected with an inducible *LIN28B* overexpression construct that was partially repressed by TetR. Cells were harvested after 72 h with and without doxycycline. (**f**) MTT-assay of cells treated with control SHC002 or *LIN28B* B6 shRNA for 144 h. SK-N-BE cells with inducible *MYCN* expression (SK-N-BE-MYCN) with and without doxycycline treatment. The relative cell viability compared to cells transfected with control SHC002 is indicated. (**g**) Protein blot of MYCN in Kelly cells 72 h after transfection with let-7a mimics, anti-let-7a or a negative control oligonucleotide (NC). (**h**) let-7a directly targets *MYCN*, resulting in reduced luciferase activity of the *MYCN* reporter construct. The effect was abrogated when the let-7a–binding site was mutated (psiCHECK-2–mut-*MYCN*). (**i**) MTS assays 1–4 d after transfection of Kelly cells with let-7a or scrambled control oligonucleotide (NC). NT, not treated. (**j**) Clonogenic assay of Kelly cells transfected with let-7a or negative control oligonucleotide 14 d after transfection. Colony counts are shown as percentage of the colonies obtained after transfection with the negative control oligonucleotide (NC). Error bars in **a**,**b**,**f**,**h**–**j** represent s.d. from three independent assays.

let-7 miRNAs regulate *MYCN* translation

Our analyses showed that LIN28B downregulates *let-7* miRNA expression and upregulates MYCN protein, suggesting that *let-7* downregulation is directly responsible for MYCN upregulation. Indeed, the *MYCN* 3′ UTR has two predicted let-7a binding sites. To experimentally test this interaction, let-7a mimics were transfected into the neuroblastoma cell lines Kelly, SK-N-BE and IMR-32 and were found to decrease MYCN protein expression. Conversely, transfection with a let-7a antagonist miRNA (antagomiR) led to higher levels of MYCN protein in Kelly cells (**Fig. 3g** and **Supplementary Fig. 13**). The effect of let-7a on MYCN expression was attenuated compared to the effect of *LIN28B* knockdown on MYCN, which could be caused by technical differences between the assays (transient lipofection with let-7a miRNAs compared to lentiviral transfection with *LIN28B*-directed shRNAs). In addition, LIN28B regulates several *let-7* family miRNA genes, which could exert a stronger effect on MYCN expression than overexpression of let-7a alone. Of note, *MYCN* mRNA levels did not change after exposure to let-7a mimics (**Supplementary Fig. 13**), which is in line with the unchanged *MYCN* mRNA levels seen with targeted silencing of *LIN28B*. These findings suggest that the accumulation of MYCN protein is inhibited by let-7 miRNAs at the translational level. To show a direct interaction between let-7a miRNA and *MYCN*, we used luciferase plasmid reporter constructs containing either the wild-type 3′ UTR from *MYCN* or the 3′ UTR with a mutated let-7a–binding sequence[43]. Transfection with let-7a mimics caused a significant decrease in reporter activity from the wild-type construct but not from the mutant construct (**Fig. 3h**). To study the phenotypic effects of the let-7a mimics, we performed methylthiazolyldiphenyl-sulfophenyltetrazoliumbromide (MTS) assays on Kelly cells, which indicated significantly decreased cell viability of cells receiving the let-7a mimics relative to those transfected with a scrambled oligonucleotide (**Fig. 3i**). In addition, colony-forming assays showed a strong decrease in the number and size of new colonies (**Fig. 3j** and **Supplementary Fig. 13**). We conclude that let-7 can directly inhibit MYCN protein translation, thereby decreasing cell viability.

LIN28B drives proliferation in non-malignant neuroblasts

Targeted knockdown of *LIN28B* inhibited proliferation and resulted in neuronal differentiation (**Fig. 2**). Overexpression in neuroblastoma cells with low expression of *LIN28B* enhanced proliferation (**Supplementary Fig. 14a**). To evaluate the oncogenic potential of *LIN28B* overexpression in non-malignant cells, we used mouse JoMa1 neuroblasts. JoMa1 cells express moderate levels of a 4-hydroxytamoxifen (4-OHT)-inducible ER-MYC fusion transgene, and these cells maintain a proliferative phenotype when cultured with 4-OHT[44]. Withdrawal of 4-OHT results in the exclusion of estrogen rector (ER)-MYC fusion proteins from the nucleus, resulting in differentiation in the presence of appropriate differentiation medium. To explore the role of LIN28B in neuroblast proliferation, we overexpressed either human *LIN28B*, *MYCN* or *GFP* (negative control) in JoMa1 cells. After withdrawal of 4-OHT, *LIN28B* and *MYCN* expression maintained proliferation in these neuroblasts (**Fig. 4a** and **Supplementary Fig. 14**). Overexpression of *LIN28B* in JoMa1 cells repressed expression of *let-7* family members and induced expression of endogenous N-myc, whereas expression of *MYCN* did not result in expression of *LIN28B* (**Fig. 4b**,**c**). Of note, in JoMa1 cells transfected with expression constructs for *LIN28B* or *MYCN*, expression of endogenous C-myc was suppressed (**Fig. 4b**). It has previously been shown that MYCN suppresses *C-myc* expression[30]. Therefore, C-myc suppression suggests that N-myc or MYCN is indeed functional in *LIN28B* or *MYCN* transfected JoMa1 cells. In addition, the gene expression patterns that were induced by expression of ectopic *LIN28B* and N-myc showed substantial overlap, suggesting that the effects of LIN28B are mainly due to its induction of endogenous N-myc (**Supplementary Fig. 14** and **Supplementary Table 6**). High *LIN28B* expression therefore maintains the proliferative capacity of primary neuroblasts and induces endogenous N-myc expression.

Lin28b-transgenic mice develop neuroblastoma

Although neuroblastomas frequently overexpress LIN28B and sometimes show amplification of the *LIN28B* gene, these data do not necessarily implicate a rate-limiting role for LIN28B in neuroblastoma pathogenesis. We therefore generated a mouse model with neural crest–specific overexpression of Lin28b. Mouse *Lin28b* was cloned downstream of a CAG promoter and a *loxP*-flanked strong transcriptional termination site and upstream of an internal ribosome entry site (IRES) and a luciferase gene (**Supplementary Fig. 15**). This construct LSL-*Lin28b* was introduced into the *Rosa26* locus by recombinase-mediated cassette exchange (RCME), and mice were generated by tetraploid injection (**Supplementary Fig. 15**). Crossbreeding of these mice with *Dbh*-iCre transgenic mice[45] resulted in deletion of the transcriptional termination site upstream of the *Lin28b* allele at the *Rosa26* locus in cells that express *Dbh* (**Supplementary Fig. 15**), thereby allowing CAG-driven expression of *Lin28b* in cells of the sympathoadrenergic lineage of the neural crest. While no mice transgenic for either *Dbh*-iCre or LSL-*Lin28b* developed any tumors, 4 out of 16 *Dbh*-iCre; LSL-*Lin28b* double-transgenic mice developed palpable abdominal tumors at ages 36–56 d. *In vivo* bioluminescence imaging (BLI) showed that these tumors were positive for luciferase activity, which indicates expression of the transgene (**Fig. 5a**). Dissection showed that one mouse had a unilateral tumor originating from the left adrenal, whereas the three others had

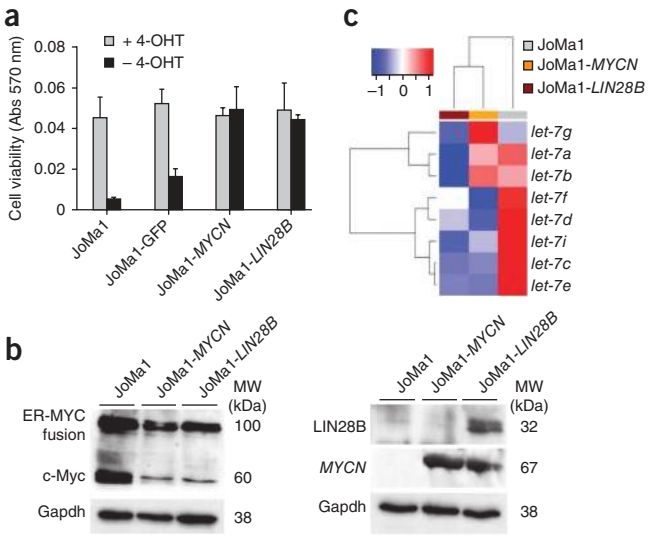

Figure 4 LIN28B drives malignant transformation. (**a**) MTT assay quantification of cell viability with and without the addition of 4-OHT. Cells were seeded at 1,000 cells per well in 96-well plates, and 4-OHT was withdrawn. After 72 h, cell viability was measured by MTT assay. Abs, absorbance. Error bars, s.d. from three independent assays. (**b**) Protein blot analysis of NMYC, LIN28B, endogenous c-Myc and ectopic ER-MYC fusion protein in JoMa1 cells treated with 4-OHT and JoMa1-*MYCN* or JoMa1-*LIN28B* cells in the absence of 4-OHT. Note that upregulation of endogenous N-myc (JoMa1-*LIN28B*) or ectopic expression of MYCN (JoMa1-*MYCN*) suppresses endogenous C-myc. In contrast, ectopic MYCN expression did not induce LIN28B. MW, molecular weight. (**c**) Stem-loop qRT-PCR was used to analyze the expression of the *let-7* family in JoMa1 cells treated with 4-OHT and JoMa1-*LIN28B* and JoMa1-*MYCN* cells in the absence of 4-OHT. All analyzed miRNAs of the *let-7* family were absent in JoMa1-*LIN28B* cells in contrast to JoMa1 and JoMa1-*MYCN* cells.

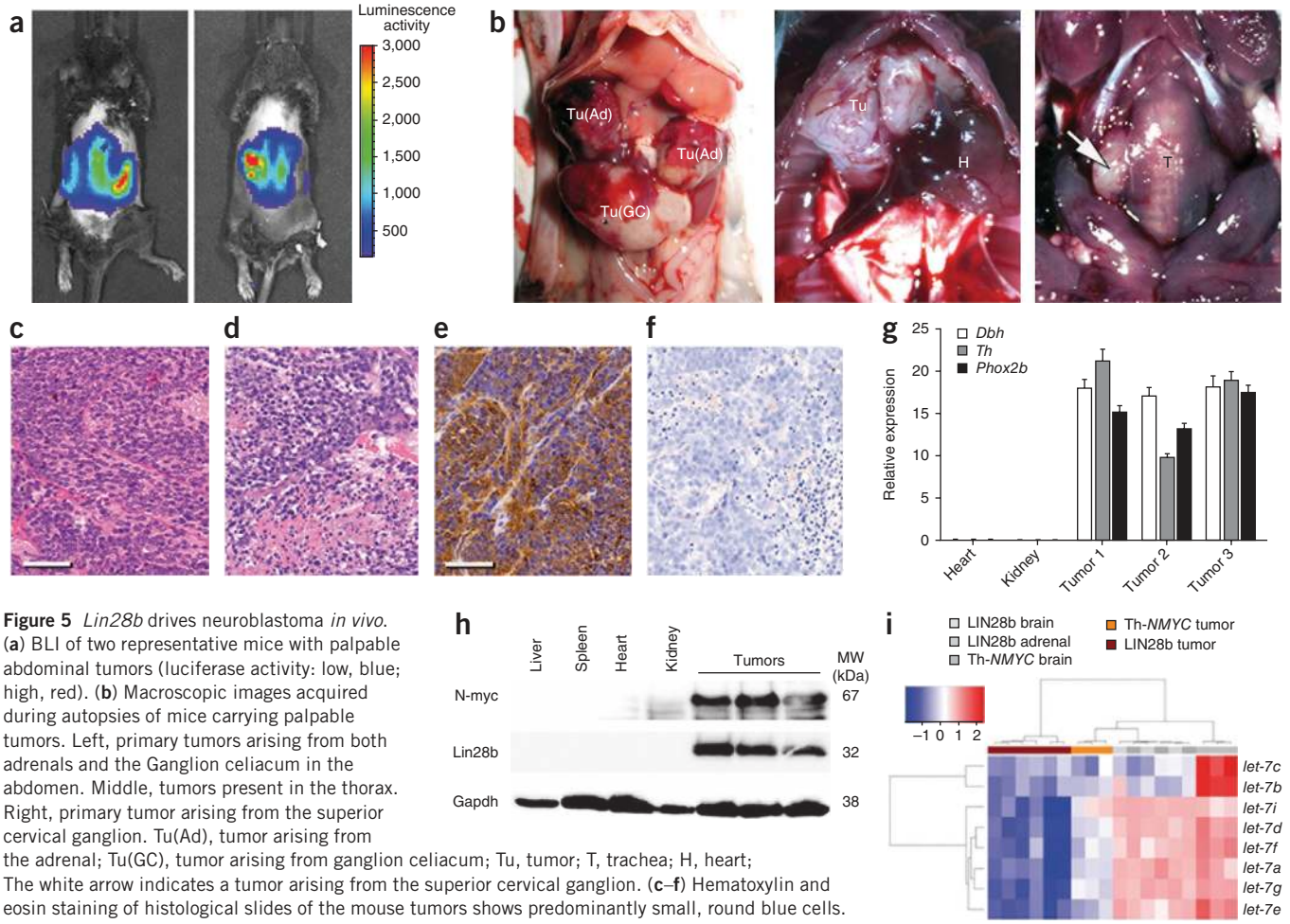

Figure 5 *Lin28b* drives neuroblastoma *in vivo*. (**a**) BLI of two representative mice with palpable abdominal tumors (luciferase activity: low, blue; high, red). (**b**) Macroscopic images acquired during autopsies of mice carrying palpable tumors. Left, primary tumors arising from both adrenals and the Ganglion celiacum in the abdomen. Middle, tumors present in the thorax. Right, primary tumor arising from the superior cervical ganglion. Tu(Ad), tumor arising from the adrenal; Tu(GC), tumor arising from ganglion celiacum; Tu, tumor; T, trachea; H, heart; The white arrow indicates a tumor arising from the superior cervical ganglion. (**c**–**f**) Hematoxylin and eosin staining of histological slides of the mouse tumors shows predominantly small, round blue cells. Note the presence of neuropil (**c**) and septae (**d**). Immunohistochemistry (IHC) confirmed Th expression in the neuroblastic tumor cell cytoplasm (**e**). Negative IHC staining control using only the secondary antibody (for Th specificity) (**f**). Scale bars, 50 μm. (**g**) qRT-PCR confirmed expression of the neuroblastoma marker genes *Dbh*, *Th* and *Phox2b* in tumor tissue but not in the control tissues. Error bars, s.d. from three independent assays. (**h**) Protein blot analysis confirmed the expression of Lin28b and N-myc in tumors compared to various control tissues. (**i**) Stem-loop qRT-PCR was used to analyze the expression of *let-7* family miRNAs. All analyzed miRNAs of the *let-7* family were absent in mouse tumors driven by Lin28b compared to adrenals or brain from LSL-*Lin28b* littermate controls or brain or neuroblastomas derived from *Th-MYCN* transgenic mice.

tumors in both adrenal glands and in the Ganglion celiacum (**Fig. 5b**). As >50% of primary human neuroblastomas also originate in the adrenal medulla, the sites of the mouse tumors are highly consistent with the primary sites of human neuroblastoma. In addition, two mice carried thoracal tumors, and three mice showed hypertrophy or tumors of the superior cervical ganglion (SCG) (**Fig. 5b**). Thus, the pattern of disease in the *Dbh*-iCre; LSL-*Lin28b* mice exactly recapitulates the spectrum of primary sites of human neuroblastoma. Tumors consisted almost entirely of small, round blue cells, similar to the histology of human neuroblastomas (**Fig. 5c**–**f**). All analyzed tumors highly expressed the neuroblastoma markers dopamine β hydoxylase (Dbh), tyrosine hydroxylase (Th) and Phox2b (paired-like homeobox 2b), as shown by qRT-PCR or immunohistochemistry (**Fig. 5c**–**g**). Taken together, the macroscopic appearance, sites of primary tumors, histology and marker gene expression unambiguously confirm that the tumors that developed in our model system are neuroblastomas. To formally prove that the tumors observed in our model system are fully transformed, malignant tumors, small pieces of tissue from two tumors originating from the adrenals were minced and injected intraperitoneally into immunocompromised nude mice. These mice developed multiple abdominal lesions resembling the primary tumors (**Supplementary Fig. 16**).

The analyses of LIN28B function in human neuroblastoma cell lines predict an essential role for LIN28B in the regulation of MYCN protein expression. We therefore investigated this aspect in the mouse tumors. In contrast to normal tissue derived from the transgenic mice, deletion of the transcriptional termination site upstream of the *Lin28b* allele was detected in all analyzed primary tumors (**Supplementary Fig. 17**). Consistently, the Lin28b protein was highly expressed in tumors but not in normal tissues from transgenic mice (**Fig. 5h**). Expression of *let-7* family members was considerably downregulated compared to normal mouse tissues (**Fig. 5i** and **Supplementary Fig. 18**). Notably, the amount of N-myc protein was very high in the *Lin28b*-transgene driven tumors (**Fig. 5h**), even compared to MYCN expression levels in tumors derived from *MYCN*-transgenic mice[46] (**Supplementary Fig. 19**). Unsupervised hierarchical clustering of mRNA expression profiles obtained from normal adrenals and tumors derived from *Dbh*-iCre; LSL-*Lin28b* or *Th-MYCN* mice revealed distinct clustering of normal adrenal medulla, *Lin28b*-transgene driven tumors and *MYCN* transgene-driven tumors. However, *Lin28b*- and *MYCN* transgene-driven neuroblastomas were more similar to each other than to normal adrenal tissue. Consistently, the mRNA expression patterns of *Lin28b*- and *MYCN*

transgene-driven mouse neuroblastomas showed significant overlap (hypergeometric test *P* value = 0), and both entities highly expressed MYCN target genes (**Supplementary Fig. 20**). Again, this suggests that Lin28b exerts most of its effect in neuroblastoma through upregulation of N-myc. To finally address the question of whether *Lin28b* transgene-driven neuroblastomas are addicted to N-myc, we used the bromodomain inhibitor JQ1, a compound that downregulates expression of N-myc as well as suppresses N-myc-driven transcription[47], to treat *Lin28b* transgene-driven mouse neuroblastomas *in vivo*. Treatment with JQ1 resulted in downregulation of endogenous N-myc protein, considerable cell death and reduced proliferation relative to untreated tumors (**Supplementary Fig. 21**).

Taken together, these experiments not only suggest that the induction of N-myc by Lin28b has a key role in the development of mouse neuroblastoma but show that MYCN is a key target of LIN28B in neuroblastoma and that targeting MYCN provides a potential therapeutic option for treatment of LIN28B-driven neuroblastomas.

DISCUSSION

In this manuscript, we describe how complex signaling involving LIN28B, let-7 and MYCN contributes to oncogenesis in pediatric neuroblastoma tumors (**Supplementary Fig. 22**). High-level amplifications of the 6q21 region including the *LIN28B* gene occur at a low frequency, and LIN28B is frequently overexpressed in high-risk neuroblastoma. Cell line analyses showed that LIN28B repressed *let-7* miRNA expression, resulting in a strong increase in the amount of MYCN protein. LIN28B expression sustains proliferation and an undifferentiated phenotype in neuroblastoma tumor cells as well as non-malignant neuroblasts. The induction of neuroblastoma in *Lin28b*-transgenic mice provides conclusive evidence of an oncogenic role for *LIN28B*.

LIN28B overexpression resulted from genomic amplification in only a few samples, as the large majority of neuroblastomas have extensive overexpression without genomic aberrations. Whole-genome sequencing of 87 neuroblastoma tumors that was recently published by our group did not show any potential activating mutations or structural aberrations in the *LIN28B* coding sequence (in addition to the already reported amplifications) or in its putative promoter regions. The increased LIN28B expression might therefore result from epigenetic changes such as altered methylation or histone modification or the deregulation of upstream processes. We observed a significant inverse correlation between *miR-125b* and *LIN28B* in our neuroblastoma tumor series. Indeed, *miR-125b* was reported to mediate LIN28B inhibition[48,49]. We confirmed a direct interaction and inhibition of LIN28B by *miR-125b*, which is located in the 11q23 region that is frequently deleted in neuroblastoma cells.

Notably, let-7 family miRNAs themselves are also known to target *LIN28B* (ref. 50). A feed-forward loop is thus created, where LIN28B accelerates its own protein expression via inhibition of *let-7* miRNAs. Most notably, the genes for several *let-7* miRNAs are located in genomic regions that are frequently deleted in neuroblastoma tumors (for example, the genes for *let-7a-2* at 11q24 and *let-7g* at 3p21). This potentially adds to the number of genomic aberrations in neuroblastoma that might drive the LIN28B-*let-7*-MYCN cascade.

Also, MYCN itself has been suggested to induce *LIN28B* transcription, which would create an even stronger feed-forward mechanism[51,52]. However, we could not detect regulation of LIN28B after modulation of MYCN using overexpression and silencing in various neuroblastoma cell line models (**Supplementary Fig. 23**), JoMa1 neural crest cells (**Fig. 4b**) and tumors derived from *Th-MYCN* mice, which, notably did not express Lin28b in most cases (**Supplementary Fig. 19** and data not shown). Therefore, it seems unlikely that transcriptional regulation of *LIN28B* by MYCN has a role in neuroblastoma.

As we showed in several of our model systems that MYCN does not induce LIN28B, MYCN is clearly a LIN28B downstream target in the LIN28B–let-7–MYCN axis in neuroblastoma (as outlined in **Supplementary Fig. 22**). We provide further evidence that MYCN is downstream of LIN28B by rescuing the phenotypic effect of *LIN28B* knockdown in two different model systems by ectopic expression of a *MYCN* transgene that is resistant to regulation by LIN28B because it lacks UTR sequences. Expression profiling of JoMa1 cells ectopically expressing *LIN28B* and *Lin28b* transgene-driven mouse neuroblastomas revealed extensive overlap with gene expression in JoMa1 cells ectopically expressing MYCN and *MYCN*-driven mouse neuroblastomas, respectively. Finally, treatment of *Lin28b* transgene-driven mouse neuroblastomas with the MYCN-inhibitory compound JQ1 induced tumor regression, again showing that N-myc is downstream of *LIN28B* and that these Lin28b-driven tumors were indeed addicted to N-myc. Taken together, these experiments indicate that LIN28B exerts most of its phenotypic effects through induction of MYCN.

Of note, our results are not restricted to *MYCN*-amplified tumors. We also detected substantial expression of *LIN28B* in neuroblastomas without *MYCN* amplification, and high expression of *LIN28B* is an adverse prognostic factor independent of *MYCN* amplification. In high-stage neuroblastoma with *MYCN* amplification, the presence of an expression signature of *MYCN* and/or MYC target genes is correlated with adverse outcome, with some of these tumors overexpressing *MYC* rather than *MYCN*[30]. We hypothesize that LIN28B also induces MYC in these tumors, and we indeed showed regulation of MYC in neuroblastoma cell lines (**Supplementary Fig. 24**). In addition, LIN28B might also induce and contribute to MYCN protein expression in high-risk neuroblastomas lacking *MYCN* amplification that do not express *MYC* but instead *MYCN* mRNA.

Recently, we showed by whole-genome sequencing of neuroblastoma that genes functioning in neuritogenesis are frequently mutated[53]. High MYCN expression in neuroblastoma has previously been associated with suppression of neuronal differentiation[54]. Our results suggest that LIN28B also suppresses differentiation leading to a neuroendocrine fate. Other authors have shown a functional relationship between LIN28B and neuronal differentiation or neurogliogenesis[4,55,56]. Therefore, we hypothesize that the increased LIN28B expression in neuroblastoma cells blocks further differentiation into mature sympathetic nerve cells. These cells thereby retain their blastic state, which encompasses many characteristics of malignant cells.

Elucidation of the full LIN28B–let-7–MYCN axis and its role in sustaining proliferation, cell viability and suppression of differentiation of neuroblasts might offer new opportunities for pharmacological intervention and new therapeutic approaches for neuroblastoma.

URLs. Gene Expression Omnibus (GEO), http://www.ncbi.nlm.nih.gov/geo/; publically available bioinformatics platform for mRNA analysis from the Department of Oncogenomics at the University of Amsterdam, http://r2.amc.nl/.

METHODS

Methods and any associated references are available in the online version of the paper.

Accession codes. Affymetrix microarray profiling results for the cohort of 88 neuroblastoma have been deposited at the Gene Expression Omnibus (GEO) under accession GSE16476.

Note: Supplementary information is available in the online version of the paper.

ACKNOWLEDGMENTS

We kindly thank A. Odersky, L. Schild, I. van der Ploeg, E. Dolman, T. Eleveld and L. Bate Eya for excellent technical assistance. The research reported in this manuscript was supported by grants from the Villa Joep Foundation, Kinderen Kankervrij (KiKa), the Tom Voûte Fund and the Netherlands Cancer Foundation. R.L.S. was a recipient of grants from the Science Foundation Ireland (07/IN.1/B1776), the Children's Medical and Research Foundation and the US National Institutes of Health (5R01CA127496). A.E. is funded by the European Union (ENCCA: EU Seventh Framework Programme, Network of Excellence 261474; ASSET: EU Seventh Framework Programme, CP 259348). Support was also provided by the National Genome Research Network (NGFNplus (Germany); PKN-01GS0894-6 to J.H.S., A.E. and A.S.) and the German Cancer Aid (grant 108941 to J.H.S. and A.E.).

AUTHOR CONTRIBUTIONS

J.J.M. and J.H.S. contributed to project coordination, data analysis and preparation of the manuscript. R.D.-F. and R.L.S. performed experiments and data analysis and contributed to preparation of the manuscript. J.K. and R. Volckmann performed analysis of bioinformatics data. M.E.E., S.L., K.D., P.M., P.v.S., J.v.N., M.B., I.B., L.J.V., F.H., K.K. and L.K.-H. conducted wet-lab experiments and data analysis. L.H., A. Sprüssel, T.T. and J.V. performed studies of the *in vivo* models. M.M.v.N., L.V., F.S. and M.F. contributed and/or organized samples and their accompanying clinical data. A. Schramm, A.E., H.N.C. and R. Versteeg supervised the project and contributed to the preparation of the manuscript.

COMPETING FINANCIAL INTERESTS

The authors declare no competing financial interests.

Published online at http://www.nature.com/doifinder/10.1038/ng.2436.
Reprints and permissions information is available online at http://www.nature.com/reprints/index.html.

1. Moss, E.G., Lee, R.C. & Ambros, V. The cold shock domain protein LIN-28 controls developmental timing in *C. elegans* and is regulated by the *lin-4* RNA. *Cell* **88**, 637–646 (1997).
2. West, J.A. *et al.* A role for Lin28 in primordial germ-cell development and germ-cell malignancy. *Nature* **460**, 909–913 (2009).
3. Polesskaya, A. *et al.* Lin-28 binds IGF-2 mRNA and participates in skeletal myogenesis by increasing translation efficiency. *Genes Dev.* **21**, 1125–1138 (2007).
4. Balzer, E., Heine, C., Jiang, Q., Lee, V.M. & Moss, E.G. LIN28 alters cell fate succession and acts independently of the *let-7* microRNA during neurogliogenesis *in vitro*. *Development* **137**, 891–900 (2010).
5. Zhu, H. *et al.* The *Lin28/let-7* axis regulates glucose metabolism. *Cell* **147**, 81–94 (2011).
6. Yu, J. *et al.* Induced pluripotent stem cell lines derived from human somatic cells. *Science* **318**, 1917–1920 (2007).
7. Viswanathan, S.R. *et al.* Lin28 promotes transformation and is associated with advanced human malignancies. *Nat. Genet.* **41**, 843–848 (2009).
8. Guo, Y. *et al.* Identification and characterization of lin-28 homolog B (LIN28B) in human hepatocellular carcinoma. *Gene* **384**, 51–61 (2006).
9. Wang, Y.C. *et al.* Lin-28B expression promotes transformation and invasion in human hepatocellular carcinoma. *Carcinogenesis* **31**, 1516–1522 (2010).
10. Permuth-Wey, J. *et al. LIN28B* polymorphisms influence susceptibility to epithelial ovarian cancer. *Cancer Res.* **71**, 3896–3903 (2011).
11. King, C.E. *et al. LIN28B* promotes colon cancer progression and metastasis. *Cancer Res.* **71**, 4260–4268 (2011).
12. Ong, K.K. *et al.* Genetic variation in *LIN28B* is associated with the timing of puberty. *Nat. Genet.* **41**, 729–733 (2009).
13. Sulem, P. *et al.* Genome-wide association study identifies sequence variants on 6q21 associated with age at menarche. *Nat. Genet.* **41**, 734–738 (2009).
14. Viswanathan, S.R., Daley, G.Q. & Gregory, R.I. Selective blockade of microRNA processing by Lin28. *Science* **320**, 97–100 (2008).
15. Lee, Y., Jeon, K., Lee, J.T., Kim, S. & Kim, V.N. MicroRNA maturation: stepwise processing and subcellular localization. *EMBO J.* **21**, 4663–4670 (2002).
16. Lee, Y. *et al.* The nuclear RNase III Drosha initiates microRNA processing. *Nature* **425**, 415–419 (2003).
17. Newman, M.A., Thomson, J.M. & Hammond, S.M. Lin-28 interaction with the Let-7 precursor loop mediates regulated microRNA processing. *RNA* **14**, 1539–1549 (2008).
18. Piskounova, E. *et al.* Determinants of microRNA processing inhibition by the developmentally regulated RNA-binding protein Lin28. *J. Biol. Chem.* **283**, 21310–21314 (2008).
19. Heo, I. *et al.* Lin28 mediates the terminal uridylation of let-7 precursor microRNA. *Mol. Cell* **32**, 276–284 (2008).
20. Piskounova, E. *et al.* Lin28A and Lin28B inhibit let-7 microRNA biogenesis by distinct mechanisms. *Cell* **147**, 1066–1079 (2011).
21. Roush, S. & Slack, F.J. The *let-7* family of microRNAs. *Trends Cell Biol.* **18**, 505–516 (2008).
22. Lee, Y.S. & Dutta, A. The tumor suppressor microRNA *let-7* represses the HMGA2 oncogene. *Genes Dev.* **21**, 1025–1030 (2007).
23. Kumar, M.S., Lu, J., Mercer, K.L., Golub, T.R. & Jacks, T. Impaired microRNA processing enhances cellular transformation and tumorigenesis. *Nat. Genet.* **39**, 673–677 (2007).
24. Johnson, C.D. *et al.* The *let-7* microRNA represses cell proliferation pathways in human cells. *Cancer Res.* **67**, 7713–7722 (2007).
25. Boyerinas, B., Park, S.M., Hau, A., Murmann, A.E. & Peter, M.E. The role of let-7 in cell differentiation and cancer. *Endocr. Relat. Cancer* **17**, F19–F36 (2010).
26. Takamizawa, J. *et al.* Reduced expression of the *let-7* microRNAs in human lung cancers in association with shortened postoperative survival. *Cancer Res.* **64**, 3753–3756 (2004).
27. Shell, S. *et al.* Let-7 expression defines two differentiation stages of cancer. *Proc. Natl. Acad. Sci. USA* **104**, 11400–11405 (2007).
28. Øra, I. & Eggert, A. Progress in treatment and risk stratification of neuroblastoma: impact on future clinical and basic research. *Semin. Cancer Biol.* **21**, 217–228 (2011).
29. Maris, J.M., Hogarty, M.D., Bagatell, R. & Cohn, S.L. Neuroblastoma. *Lancet* **369**, 2106–2120 (2007).
30. Westermann, F. *et al.* Distinct transcriptional MYCN/c-MYC activities are associated with spontaneous regression or malignant progression in neuroblastomas. *Genome Biol.* **9**, R150 (2008).
31. Bray, I. *et al.* Widespread dysregulation of miRNAs by *MYCN* amplification and chromosomal imbalances in neuroblastoma: association of miRNA expression with survival. *PLoS ONE* **4**, e7850 (2009).
32. De Preter, K. *et al.* miRNA expression profiling enables risk stratification in archived and fresh neuroblastoma tumor samples. *Clin. Cancer Res.* **17**, 7684–7692 (2011).
33. Shohet, J.M. *et al.* A genome-wide search for promoters that respond to increased MYCN reveals both new oncogenic and tumor suppressor microRNAs associated with aggressive neuroblastoma. *Cancer Res.* **71**, 3841–3851 (2011).
34. Schulte, J.H. *et al.* MYCN regulates oncogenic microRNAs in neuroblastoma. *Int. J. Cancer* **122**, 699–704 (2008).
35. Ma, L. *et al.* miR-9, a MYC/MYCN-activated microRNA, regulates E-cadherin and cancer metastasis. *Nat. Cell Biol.* **12**, 247–256 (2010).
36. Lovén, J. *et al.* MYCN-regulated microRNAs repress estrogen receptor-α (ESR1) expression and neuronal differentiation in human neuroblastoma. *Proc. Natl. Acad. Sci. USA* **107**, 1553–1558 (2010).
37. Tivnan, A. *et al.* MicroRNA-34a is a potent tumor suppressor molecule *in vivo* in neuroblastoma. *BMC Cancer* **11**, 33 (2011).
38. Le, M.T. *et al.* MicroRNA-125b promotes neuronal differentiation in human cells by repressing multiple targets. *Mol. Cell. Biol.* **29**, 5290–5305 (2009).
39. Cole, K.A. *et al.* A functional screen identifies *miR-34a* as a candidate neuroblastoma tumor suppressor gene. *Mol. Cancer Res.* **6**, 735–742 (2008).
40. Welch, C., Chen, Y. & Stallings, R.L. MicroRNA-34a functions as a potential tumor suppressor by inducing apoptosis in neuroblastoma cells. *Oncogene* **26**, 5017–5022 (2007).
41. Buechner, J. *et al.* Tumour-suppressor microRNAs *let-7* and *mir-101* target the proto-oncogene *MYCN* and inhibit cell proliferation in *MYCN*-amplified neuroblastoma. *Br. J. Cancer* **105**, 296–303 (2011).
42. Molenaar, J.J. *et al.* Copy number defects of G1-cell cycle genes in neuroblastoma are frequent and correlate with high expression of E2F target genes and a poor prognosis. *Genes Chromosom. Cancer* **51**, 10–19 (2012).
43. Huntzinger, E. & Izaurralde, E. Gene silencing by microRNAs: contributions of translational repression and mRNA decay. *Nat. Rev. Genet.* **12**, 99–110 (2011).
44. Schulte, J.H. *et al.* MYCN and ALKF1174L are sufficient to drive neuroblastoma development from neural crest progenitor cells. *Oncogene* published online, doi:10.1038/onc.2012.106 (9 April 2012).
45. Stanke, M. *et al.* Target-dependent specification of the neurotransmitter phenotype: cholinergic differentiation of sympathetic neurons is mediated *in vivo* by gp 130 signaling. *Development* **133**, 141–150 (2006).
46. Weiss, W.A., Aldape, K., Mohapatra, G., Feuerstein, B.G. & Bishop, J.M. Targeted expression of MYCN causes neuroblastoma in transgenic mice. *EMBO J.* **16**, 2985–2995 (1997).
47. Mertz, J.A. *et al.* Targeting MYC dependence in cancer by inhibiting BET bromodomains. *Proc. Natl. Acad. Sci. USA* **108**, 16669–16674 (2011).
48. Liang, L. *et al.* MicroRNA-125b suppressesed human liver cancer cell proliferation and metastasis by directly targeting oncogene *LIN28B2*. *Hepatology* **52**, 1731–1740 (2010).
49. Wang, J. *et al.* MicroRNA-125b/Lin28 pathway contributes to the mesendodermal fate decision of embryonic stem cells. *Stem Cells Dev.* **21**, 1524–1537 (2012).
50. Rybak, A. *et al.* A feedback loop comprising *lin-28* and *let-7* controls pre-*let-7* maturation during neural stem-cell commitment. *Nat. Cell Biol.* **10**, 987–993 (2008).
51. Helland, Å. *et al.* Deregulation of *MYCN*, *LIN28B* and *LET7* in a molecular subtype of aggressive high-grade serous ovarian cancers. *PLoS ONE* **6**, e18064 (2011).
52. Cotterman, R. & Knoepfler, P.S. N-Myc regulates expression of pluripotency genes in neuroblastoma including *lif*, *klf2*, *klf4*, and *lin28b*. *PLoS ONE* **4**, e5799 (2009).
53. Molenaar, J.J. *et al.* Sequencing of neuroblastoma identifies chromothripsis and defects in neuritogenesis genes. *Nature* **483**, 589–593 (2012).
54. Valentijn, L.J. *et al.* Inhibition of a new differentiation pathway in neuroblastoma by copy number defects of *N-myc*, *Cdc42*, and *nm23* genes. *Cancer Res.* **65**, 3136–3145 (2005).
55. Eda, A., Tamura, Y., Yoshida, M. & Hohjoh, H. Systematic gene regulation involving miRNAs during neuronal differentiation of mouse P19 embryonic carcinoma cell. *Biochem. Biophys. Res. Commun.* **388**, 648–653 (2009).
56. Olsson-Carter, K. & Slack, F.J. A developmental timing switch promotes axon outgrowth independent of known guidance receptors. *PLoS Genet.* **6** pii: e1001054 (2010).

ONLINE METHODS

Material and data from human subjects. Primary tumor samples were surgically derived from untreated individuals with neuroblastoma and were immediately frozen in liquid nitrogen. Affymetrix expression data from tumors and normal tissues in adults was derived from the Expression Project for Oncology (EXPO) database from the International Genomics Consortium (IGC).

DNA isolation, Southern blotting and aCGH analysis. High-molecular-weight DNA was extracted from tumor tissue using standard procedures[57]. Southern blot analysis was performed as previously described[58]. Hybridization probes were generated using PCR with primers targeting the 6q21 region. aCGH using a custom 44K or 66K Agilent aCGH chip, enriched for key regions of loss and/or gain for neuroblastoma (at 10-kb resolution), miRNAs/transcribed ultra-conserved regions (T-UCRs) and cancer gene census genes, was performed as described previously[59].

RNA isolation and Affymetrix mRNA profiling and data analysis. Total RNA from tumors and cell lines was extracted using TRIzol reagent (Invitrogen) or miRNeasy kit (Qiagen), following the manufacturer's protocol. RNA concentration and quality were determined using the RNA 6000 Nano assay on the Agilent 2100 Bioanalyzer (Agilent Technologies). Fragmentation of cRNA, hybridization to hg-u133 plus 2.0, Exon St 1.0 arrays or Murine Genome 430 2.0 microarrays and scanning were carried out according to the manufacturer's protocol (Affymetrix). Expression data were normalized with the MAS5.0 algorithm within the Gene Chip Operating Software (GCOS) program from Affymetrix. Target intensity was set to 100. All data were analyzed using the R2 web application. To asses whether the amount of overlap between genes differentially expressed in mouse tumors induced by *MYCN* transgene versus normal adjacent tissue and tumors induced by *LIN28B* transgene versus normal adjacent tissue was more prominent than expected, Venn diagram data were collected, and hypergeometric tests were performed. In the JoMa1 experiment, differential expression between *GFP*-expressing control samples and *LIN28B*- or *MYCN*-overexpressing cells was assessed by a GCOS two-sample analysis, applying the following restrictions: (i) expression within a comparison should exceed 100 in at least 1 sample; (ii) genes should be considered expressed in at least 1 sample (present call 1); (iii) at minimum, 1 significant change should be reported by GCOS ($P < 0.0001$); (iv) a log-fold change of at least 1 should be reported by GCOS; and (v) a gene can only be represented by 1 reporter. For the tumors from transgenic mice, differential expression was assessed by comparing three biological replicates of adrenal gland against four biological replicates for LIN28B or MYCN via empirical Bayes' analysis (limma) on those genes considered to be expressed in at least one sample (present call 1), where every gene is represented by only one reporter (hugo-once function in R2).

Multivariate analysis. Multivariate Cox regression analysis of overall survival was performed in R2.13.0 using the coxph() function as provided by the survival package. Input variables were dichotomized (alk_mutation, age_diagnosis_18months, kaplanscan_lin28b_overall, mycn_amp, INSS_hl). INSS_hl was defined as ST1,2,4s versus ST3,4. kaplanscan_LIN28B_overall was dichotomized on the basis of the cutoff obtained from the Kaplan scan on overall survival.

Cell culture and treatment. SK-N-BE, SK-N-FI, IMR-32 and NGP cells were cultured as previously described[60]. Primary references for these cell lines can be found in ref. 60. The Kelly cell lines were purchased from the European Collection of Animal Cultures and grown in RPMI-1640 supplemented with 10% FBS and 2 mM penicillin and streptomycin (GIBCO Invitrogen by Life Technologies). Cell lines were authenticated by CA repeat markers. Cell culture and experiments with JoMa1 cells were performed as previously described[44]. NHO2A cells (a mouse neuroblastoma cell line from the *Th-MYCN* mouse model) were cultured as previously described[61].

Generation and expression of plasmids. SK-N-BE, SK-N-AS and SY5Y cells were stably transfected with the pcDNA6/TR vector (Invitrogen). PCR-amplified full-length human *LIN28B* cDNA was subcloned into the pENTR/D-TOPO vector (Invitrogen). This plasmid was used in the JoMa1 experiments. Using the LR Clonase II enzyme (Invitrogen), *LIN28B* cDNA was then introduced into the pMSCVpuro vector (Clontech), in which a gateway cassette was previously introduced using the Gateway Conversion kit (Invitrogen). SK-N-BE–pTR6 cells were stably transfected with this construct to generate SK-N-BE–pTR6-*LIN28B* cells. To generate SK-N-AS–pTr6-*MYCN* cells, the coding sequence of human *MYCN* was cloned into the pcDNA4/TO/myc-His vector (Invitrogen), which was subsequently stably transfected into SK-N-AS–pTR6 cells. To generate SY5Y-pTr6-*MYCN* and SK-NB-E–pTR6-*MYCN* cells, the coding sequence of *MYCN* was cloned into the pENTR-D-TOPO vector and transferred to the pLenti4/puro/TO/V5-DEST vector with the Gateway LR Clonase II system (all from Invitrogen).

Lentivirus-mediated shRNA silencing. Lentiviral shRNA expression vectors were obtained from Sigma (MISSION shRNA Lentiviral Library), and the preparation of viral particles and infection of cells were performed as previously descirbed[62]. SK-N-BE, SK-N-FI, IMR-32 and Kelly cells were transfected with vectors expressing shRNA to human *LIN28B* (Sigma, TRCN0000122191 (B6) or TRCN0000138995 (B7)) or human *MYCN* (Sigma, TRCN0000020696) or with the control lentivirus (Sigma, Non-Target shRNA Control, SHC002).

siRNA or miRNA transfections. pre-miRNA and anti-miRNA to let-7a and miR-125b and negative control 1 (a scrambled oligonucleotide) were obtained from Ambion, and small interfering RNA (siRNA) to mouse *Lin28b* was obtained from Qiagen. siRNA was transiently transfected into NHO2A cells at a final concentration of 40 nM using 0.5 µl (96-well plate) or 5 µl (6-well plate) of the siPORT NeoFX transfection reagent (Ambion). miRNA was transiently transfected into Kelly cells at a final concentration of 30 nM using 5 µl (6-well plate) of the siPORT NeoFX transfection reagent. Cell culture medium was changed after 8 h to remove the transfection agent.

Protein blotting. For blots shown in **Figures 1–4**, cells were harvested at various time points on ice. Cells were lysed with Laemmli buffer (20% glycerol, 4% SDS, 100 mM Tris-HCl, pH 6.8, in Milli-Q). Protein was quantified by RC-DC protein assay (Bio-Rad). Lysates were separated by 10% SDS-PAGE and electroblotted onto a transfer membrane (Millipore). Blocking and incubations with antibody were performed in OBB (LI-COR), according to the manufacturer's protocol. The primary antibodies used recognized human and mouse LIN28B (Cell Signaling Technology, 4196), actin (Abcam, Ab6276), Cdk6 (Santa Cruz Biotechnology, C-21; sc-177), Total RAS (Cell Signaling Technology, 3339) and MYCN[54]. The secondary antibodies used were provided by LI-COR. Proteins were visualized with the Odyssey Bioanalyzer (LI-COR).

In the blots shown in all other figures, total protein was isolated from cells using RIPA buffer (50 mM HEPES, pH 7.4, 150 mM NaCl, 0,1% SDS, 1% Triton X-100, 1% NP-40). Protein concentration was measured using the BCA assay from Pierce. We separated 20 µg of proteins per lane by10% SDS-PAGE, and proteins were blotted onto Hybond-C membranes (Amersham, RPN303E). Membranes were probed with antibody to LIN28B (Cell Signaling Technology, 4196; 1:1,000 dilution) or NMYC (Santa Cruz Biotechnology, sc-53993; 1:500 dilution) and GAPDH (Millipore, MAB374;1:4,000 dilution) or α-tubulin (Abcam, ab7291; 1:5,000 dilution) for loading control. Signal was detected using the Immobilon Western (Millipore) or ECL Plus Western (Amersham, RPN2132) detection kit.

Cell fractionation. Protein was harvested from SK-N-BE cells and fractionated using the Subcellular Proteome Extraction kit (Novagen, 539790) according to manufacturer's protocol. Fraction I (cytosol), II (membrane/organelle) and III (nucleus) were used for protein blot analysis. Antibodies to PARP (Cell Signaling Technology, 9542) and α-tubulin (Sigma, T5168) were used for fractionation control.

Phalloidin staining. Phalloidin staining was performed as previously described[60].

Flow cytometry and cell counting. Flow cytometry and propidium iodide (PI) staining were performed as previously described[63]. Cell counting of SK-N-FI cells was performed in triplicate using a Beckman Coulter counter. SK-N-FI cells were seeded at a density of 400,000 cells per 6-cm dish 24 h

before transduction with viruses encoding shRNA. Fresh medium with 1 μg/ml puromycin was added 24 h after transduction. At 4, 7 and 10 d after transduction, cells were counted and reseeded.

MTT assays. Methyl-thiazolyldiphenyl-tetrazoliumbromide (MTT) assays were performed as previously described[64]. In brief, 200,000 cells were plated 24 h before viral transduction. Cells were virally transduced, puromycin selection was started 24 h later and cells were grown until the MTT assays were performed.

Cell proliferation assays. Cell growth was measured at designated time points using the Cell counting kit-8 (CCK-8; Dojindo Molecular Technologies) according to the manufacturer's protocol. An average of six replicates were analyzed, and statistical analysis was performed by *t* test.

Clonogenic assays. Kelly cells were transfected with pre-miRNA for *let-7a* or negative control 1 for 24 h, as previously described, and 500 cells were then seeded into a 6-well plate in triplicate. After a 15-d incubation, plates were gently washed with PBS, and colonies were fixed with ice-cold 100% methanol and stained with 0.5% crystal violet in 25% methanol. Colonies were manually counted.

Luciferase assays. To generate *MYCN* luciferase reporter vectors, a 494-bp region of the 3′ UTR of *MYCN* containing both of the predicted let-7–binding sites was inserted into the dual-luciferase psiCHECK-2 reporter vector (Promega), designated psiCHECK-2–*MYCN*. As a negative control, a complete mutation was introduced into both the let-7 seed regions of this sequence, designated psiCHECK-2–mut-*MYCN*. To generate *LIN28B* luciferase reporter vectors, a 347-bp region of the 3′ UTR of *LIN28B* containing the predicted miR-125b–binding site was inserted into the psiCHECK-2 dual-luciferase reporter vector, designated psiCHECK-2–*LIN28B*. To ensure complete disruption of the miR-125b seed sequence, a 19-nt mutation was introduced into the seed region and flanking regions, designated psiCHECK-2–mut-*LIN28B*. Kelly cells were plated in 6-well plates and were cotransfected using Lipofectamine 2000 (Invitrogen) with either 2 μg of psiCHECK-2–*MYCN* or psiCHECK-2–*LIN28B* or with the vectors encoding mutant miRNA-binding sites along with 30 nM of either the pre-miRNA for *let-7a* or *mir-125b* or with Negative Control 1. Luciferase activity was measured 48 h after transfection using the Dual-Luciferase Reporter Assay System (Promega).

mRNA qPCR. We used 1 μg of RNA isolated using TRIzol for cDNA synthesis, and 1 μl of the resulting cDNA was used for qPCR. Fluorescence-based kinetic RT-PCR was performed using the real-time iCycler (Bio-Rad) or the StepOnePlus PCR platform (Applied Biosystems) in combination with the intercalating fluorescent dye SYBR Green I. IQ SYBR Green I Supermix (Bio-Rad) was used in accordance with the manufacturer's instructions. Biogazelle software was used for data analysis. Primer sequences are provided in **Supplementary Table 7**.

miRNA qPCR. Mature miRNA expression levels were quantified using stem-loop qRT-PCR technology as described previously[65]. In brief, total RNA was reverse transcribed using the mouse or human stem-loop Megaplex RT Primer Pools (Life Technologies) with the TaqMan microRNA Reverse Transcription kit (Applied Biosystems, nr. 4366596) with respective miRNA RT primers according to the manufacturer's instructions. A limited-cycle pre-amplification step was applied (in case of multiplex analysis), and mature miRNA levels were quantified using miRNA-specific TaqMan probes (Life Technologies). Raw miRNA expression data were normalized using the global mean[66] for multiplex analysis or were normalized to *SNORD44* or *SNORA66* levels (analysis of individual miRNAs). Primer sequences are provided in **Supplementary Table 7**.

Generation of LSL-Lin28b mice. *Lin28b* cDNA was ligated into a proprietary plasmid between FLP recombinase sites compatible for RCME (Taconic-Artemis). This plasmid was transfected into B6S6F1 embryonic stem (ES) cells (Taconic-Artemis) containing F3/FLP recombinase sites compatible for RCME at the *ROSA26* locus. Recombinant clones were isolated and validated by Southern blot. Mice were generated by injection of ES cells into tetraploid blastocysts. Litters were backcrossed to 129X1/SvJ mice (Jackson Laboratory) for at least one generation and were crossbred to *Dbh*-iCre mice[45]. Mouse genotyping and confirmation of Cre-mediated recombination was performed as previously described[67]. Mice were palpated weekly for abdominal tumors and analyzed by *in vivo* luciferase imaging[68]. Primer sequences are provided in **Supplementary Table 7**.

Retrotransplantation with tumors and treatment with JQ1. Primary tumors were minced and pulled through a 20-gauge syringe. After intraperitoneal or subcutaneous injection into immunocompromised nu/nu mice, animals were palpated weekly for tumor growth. Mice were treated with JQ1 (50 mg per kg body weight) or control twice daily by intraperitoneal injection for three consecutive days when the volume of the subcutaneous tumor reached 500–1,000 mm^3, and animals were sacrificed 2 h after the last injection.

Tissue array and IHC. Tissue arrays were prepared using standard procedures. IHC was performed as previously described[60,64], using primary antibodies to tyrosine hydroxylase (Abcam, ab76442; 1:2,000 dilution), cleaved caspase-3 (Cell Signaling Technology, 9661; 1: 750 dilution), mouse Ki67 (TEC-3; Dako Cytomation, M7249; 1:50 dilution) and LIN28B (Cell Signaling Technology, 4196; 1:500 dilution).

57. Caron, H. *et al.* Allelic loss of chromosome 1p36 in neuroblastoma is of preferential maternal origin and correlates with *N-myc* amplification. *Nat. Genet.* **4**, 187–190 (1993).
58. Molenaar, J.J., van Sluis, P., Boon, K., Versteeg, R. & Caron, H.N. Rearrangements and increased expression of cyclin D1 (*CCND1*) in neuroblastoma. *Genes Chromosom. Cancer* **36**, 242–249 (2003).
59. Fieuw, A. *et al.* Identification of a novel recurrent 1q42.2–1qter deletion in high risk *MYCN* single copy 11q deleted neuroblastomas. *Int. J. Cancer* **130**, 2599–2606 (2012).
60. Molenaar, J.J. *et al.* Cyclin D1 and CDK4 activity contribute to the undifferentiated phenotype in neuroblastoma. *Cancer Res.* **68**, 2599–2609 (2008).
61. Cheng, A.J. *et al.* Cell lines from *MYCN* transgenic murine tumours reflect the molecular and biological characteristics of human neuroblastoma. *Eur. J. Cancer* **43**, 1467–1475 (2007).
62. Molenaar, J.J. *et al.* Cyclin D1 is a direct transcriptional target of GATA3 in neuroblastoma tumor cells. *Oncogene* **29**, 2739–2745 (2010).
63. Molenaar, J.J. *et al.* Inactivation of CDK2 is synthetically lethal to MYCN over-expressing cancer cells. *Proc. Natl. Acad. Sci. USA* **106**, 12968–12973 (2009).
64. Schulte, J.H. *et al.* Lysine-specific demethylase 1 is strongly expressed in poorly differentiated neuroblastoma: implications for therapy. *Cancer Res.* **69**, 2065–2071 (2009).
65. Mestdagh, P. *et al.* High-throughput stem-loop RT-qPCR miRNA expression profiling using minute amounts of input RNA. *Nucleic Acids Res.* **36**, e143 (2008).
66. Mestdagh, P. *et al.* A novel and universal method for microRNA RT-qPCR data normalization. *Genome Biol.* **10**, R64 (2009).
67. Heukamp, L.C. *et al.* Targeted expression of mutated *ALK* induces neuroblastoma in transgenic mice. *Sci. Transl. Med.* **4**, 141ra91 (2012).
68. Bill, A. *et al.* Cytohesins are cytoplasmic ErbB receptor activators. *Cell* **143**, 201–211 (2010).

doi:10.1038/ng.2436